Existence of a Proton Transfer Chain in Bacteriorhodopsin: Participation of Glu-194 in the Release of Protons to the Extracellular Surface†

Andrei K. Dioumaev,‡ Hans-Thomas Richter,‡ Leonid S. Brown,‡ Michikazu Tanio,§ Satoru Tuzi,§ Hazime Saitô,§ Yoshiaki Kimura,|| Richard Needleman,⊥ and Janos K. Lanyi*,‡

Department of Physiology & Biophysics, University of California, Irvine, California 92697-4056, Himeji Institute of Technology, Harima Science Garden City, Kamigori, Hyogo 678-12, Japan, Department of Structural Biology, Biomolecular Engineering Research Institute, Suita, Osaka 565, Japan, and Department of Biochemistry, Wayne State University, Detroit, Michigan 48201

Received July 29, 1997; Revised Manuscript Received December 16, 1997

ABSTRACT: Glu-194 near the extracellular surface of bacteriorhodopsin is indispensable for proton release to the medium upon protonation of Asp-85 during light-driven transport. As for Glu-204, its replacement with glutamine (but not aspartate) abolishes both proton release and the anomalous titration of Asp-85 that originates from coupling between the pK_a of this buried aspartate and those of the other acidic groups. Unlike the case of Glu-204, however, replacement of Glu-194 with aspartate raises the pK_a for proton release. In Fourier transform infrared spectra of the E194D mutant a prominent positive band is observed at 1720 cm^{-1}. It can be assigned from [4-^{13}C]aspartate and D_2O isotope shifts to the C═O stretch of protonated Asp-194. Its rise correlates with proton transfer from the retinal Schiff base to Asp-85. Its decay coincides with the appearance of a proton at the surface, detected under similar conditions with fluorescein covalently bound to Lys-129 and with pyranine. Its amplitude decreases with increasing pH, with a pK_a of about 9. We show that this pK_a is likely to be that of the internal proton donor to Asp-194, the Glu-204 site, before photoexcitation, while ^{13}C NMR titration indicates that Asp-194 has an initial pK_a of about 3. We propose that there is a chain of interacting residues between the retinal Schiff base and the extracellular surface. After photoisomerization of the retinal the pK_a's change so as to allow (i) Asp-85 to become protonated by the Schiff base, (ii) the Glu-204 site to transfer its proton to Asp-194 in E194D, and therefore to Glu-194 in the wild type, and (iii) residue 194 to release the proton to the medium.

Photoisomerization of the retinal in bacteriorhodopsin from all-trans to 13-cis initiates a sequence of proton transfer reactions which together add up to the net transport of a proton from the cytoplasmic to the extracellular side of the membrane (*1*−*5*). The first of these transfers is from the protonated retinal Schiff base to the anionic Asp-85 in the L to M (*6*) reaction.[1] Asp-85 remains protonated until the last step of the reaction cycle (*7*−*9*), but its protonation causes the release of a proton to the extracellular surface. It has been suggested that the source of this proton is Glu-204 (*10*, *11*). The shapes of the titration curves for Asp-85 in the dark in the wild-type and in the E204Q and E204D (as well as the D85E, D85E/E204Q, Y185F, and Y185F/E204Q) mutants have indicated that the pK_a of residue 204, or a protonatable site dependent on residue 204 ("Glu-204 site"), is coupled to the pK_a of residue 85 in such a way that near neutral pH either one or the other group is protonated but not both (*11*−*13*). The structural and energetic rationale for this may be hydrogen-bonded water which allows electrostatic interaction, probably facilitated by some structural rearrangement of Arg-82 in this region (*14*, *15*). The pK_a of the Glu-204 site is thus about 9 in the unphotolyzed protein but becomes lowered to about 5 after protonation of Asp-85. These values agree with previous estimates of the two pK_a's of the then unknown proton release group (*16*, *17*). The coupling between Asp-85 and Glu-204, as revealed by the titration behavior of Asp-85, therefore provides a rationale for both proton release and the rise of the pK_a of Asp-85 once the proton is released, preventing return of the transferred proton from Asp-85 to the Schiff base.

At the end of the photocycle, Asp-85 dissociates and is presumed to reprotonate the proton release site that is vacant. Deprotonation of Asp-85 in the mutant E204Q occurs also at this time, but it is considerably slower than in the wild type and leads to an unusually large accumulation of the O intermediate (*9*, *10*). Since proton uptake at the cytoplasmic surface is unperturbed under these conditions, the uptake occurs before the proton release. It was assumed that in E204Q the proton detected at the surface originates from Asp-85 as it recovers its initial low pK_a (*16*, *18*).

† This work was funded partly by grants from the National Institutes of Health (GM 29498 to J.K.L.), the Department of Energy (DEFG03-86ER13525 to J.K.L.), and the U.S. Army Research Office (DAAL03-92-G-0406 to R.N.).

* To whom correspondence should be addressed. E-mail: JLANYI@ORION.OAC.UCI.EDU. Fax: (714) 824-8540.

‡ University of California.

§ Himeji Institute of Technology.

|| Biomolecular Engineering Research Institute.

⊥ Wayne State University.

[1] Abbreviations: L, M, N, and O are photointermediates of bacteriorhodopsin. E204Q and other such designations refer to mutants in which the wild-type residue in single-letter code is followed by the residue number and the residue to which it is changed. FTIR is Fourier transform infrared. CP-MAS is cross polarization−magic angle spinning, DD-MAS is dipolar decoupled−magic angle spinning. Bis(Tris)-propane is 1,3-bis[[tris(hydroxymethyl)methyl]amino]propane; CAPS is 3-cyclohexylamino-1-propanesulfonic acid; MES is 2-(morpholino)-ethanesulfonic acid; pyranine is 8-hydroxy-1,3,6-pyrenetrisulfonate.

S0006-2960(97)01842-4 CCC: $15.00
Published on Web 02/03/1998

It is possible, however, that other protonatable residues in the extracellular region also participate in the proton release. Replacement of Glu-194 with cysteine is reported to inhibit proton release, much like replacement of Glu-204 with glutamine (*19*). The recent high-resolution structure obtained with electron diffraction suggested that proton release proceeds through interacting buried glutamate residues in the extracellular region, some of which are protonated while others are unprotonated at pH 5.5 (*20*). From the increased scattering of electrons at higher resolution as expected for negatively charged groups, Glu-204 was suggested to be anionic under the sample conditions. Absence of such an effect for Glu-194 suggested that this residue is protonated. In light of these results, we examined more closely the participation of Glu-9 and Glu-194, the only other buried acidic groups near the extracellular surface, in the proton release and in the proposed Asp-85/Glu-204 coupling.

Proton release in the photocycle, the titration behavior of Asp-85 in the dark, and time-resolved FTIR spectra have been measured for Glu-9 and several Glu-194 mutants. Proton release in E9A is like that in the wild type, ruling out a proton conduction pathway that passes obligatorily through this residue. The results indicate, however, that an acidic residue at position 194 is indispensable for proton release. Normal proton release does not occur in E194Q, as in E194C. Protonation of Asp-85 by the Schiff base is followed by proton transfer from the Glu-204 site to Asp-194, and after a few milliseconds' delay, the proton is released from Asp-194 to the surface where we detected it with fluorescein and pyranine. In E194D, therefore, Asp-194 is part of a proton transfer chain that leads from the retinal Schiff base to the extracellular surface. We suggest that, in the wild-type protein, Glu-194 behaves as Asp-194 in the E194D mutant except that it releases the proton more rapidly.

MATERIALS AND METHODS

Purple membranes with mutated bacteriorhodopsin were prepared from *Halobacterium salinarium* by a standard method (*21*). The E204Q and E204D mutants used have been described before (*10*). The E9A, E194D, E194Q, E194D/E204D, E194D/E204Q, E194Q/E194D, and E194Q/E204Q mutants were constructed as described elsewhere (*22*). The purple membranes were stored in about 40% sucrose, frozen at − 70 °C. Labeling of bacteriorhodopsin was with L-[4-^{13}C]aspartate purchased from Cambridge Isotope Laboratories (Andover, MA), without further purification. *H. salinarium*, containing the vector with either the wild-type or the E194D *bop* gene, was grown in the TS medium of Onishi et al. (*23*) in which unlabeled L-aspartate was replaced by [4-^{13}C]aspartate. After dialysis of the cells against a large excess of water, the purple membranes were isolated by centrifugation and suspended for storage in 5 mM HEPES at pH 7.0 containing 10 mM NaCl and 0.025% NaN_3.

The pH dependence of the absorption spectra (in dark-adapted samples) and the rate of dark adaptation were measured on a Shimadzu Model 1601 spectrophotometer connected to a desktop computer. In some cases, the membranes were encased in polyacrylamide gel, as before (*13*). The dark adaption rates shown are fits of the measured absorption changes, followed until virtually complete, to single exponentials, as before (*11*). Transient absorption changes in the photocycle were followed after photoexcitation with a Nd:YAG laser pulse (532 nm, 7 ns), as in earlier publications of ours (e.g., ref 24), except that the data were acquired with a 30 MHz analog-to-digital converter (Gage Compuscope 6012/PCI-4M card, Gage Applied Sciences, Montreal, Canada), utilizing custom software. The 4×10^6 data points collected were reductively averaged so as to provide 250 points on a logarithmic time scale. Transient pH changes were measured with either pyranine or fluorescein covalently bound to Lys-129 (*25*). In the case of pyranine (50 μM), the controls were samples without the dye; in the case of fluorescein, the controls were samples with added phosphate buffer. Where the temperature is not indicated, it was 22 °C.

Time-resolved FTIR spectra were measured on a Bruker IFS-66 (Bruker Analytische Messtechnik GmbH, Karlsruhe, Germany) step-scan spectrometer at 8 cm^{-1} resolution. The samples were prepared by drying purple membrane suspensions in distilled water, at about neutral pH, on a CaF_2 window (Harrick, Ossining, NY). The semidry films, about 10 mm in diameter, were equilibrated with an excess of buffer solution at the desired pH for at least 20 min. They were then partly dried and rehydrated with 3.5 μL of the same buffer, and a second CaF_2 window was placed onto the sample without a spacer. Once the cell was assembled, therefore, the sample squeezed between the two windows was fully and uniformly hydrated. All buffers contained 100 mM NaCl and either succinate (pH 3−4), MES (pH 5−6), phosphate (pH 7), or bis(Tris)propane (pH 8−9), all at 40 mM. The FTIR measurements were done at 15 °C unless otherwise indicated, controlled with a refrigerated water bath (RTE-111, Neslab, Portsmouth, NH) and a temperature-controlled infrared cell (Harrick, Ossining, NY). For the ^{13}C-labeled sample only, where better signal/noise in the 1600−1700 cm^{-1} region was required, the last hydration step was replaced by placing a 1 μL drop of water on the window outside the IR beam and separating the second window from the first with a 15 μm spacer.

All FTIR measurements were with an HgCdTe photovoltaic detector (KMPV11-1-LJ2/239; Kolmar Technologies, Conyers, GA). The digitized dc-coupled output of the preamplifier provided both the amplitude and the phase information for the Fourier transformation. Custom-written software provided a pretrigger for the spectrometer in such a way that for step-scan experiments the first ~60 time slices were measured *before* the excitation flash. Data from these slices were averaged and used to calculate the difference spectra. In each experiment, 10^3 time-resolved slices were recorded. To cover all of the photocycle, two separate sets of experiments—one with a *fast* time base (5 μs per time slice) and the other with a *slow* one (50−500 μs per time slice)—were performed. Slower time bases were covered with rapid-scan measurements, where the data were averaged over geometrically increasing numbers of scans. This resulted in 10−30 time slices per decade on a logarithmic time scale. The time resolution in this case was 65 ms.

Photoexcitation was with a Nd:YAG laser pulse, as above. The repetition rate of the excitation was low enough to provide spacing between flashes at least 5 times greater than the slowest time constants detected with the same samples

in visible flash photolysis experiments. To minimize light-induced sample degradation (*26*, *27*), the excitation flash intensity was kept below 3 mJ/cm^2.

The final FTIR spectra were obtained by averaging data from several separate experiments (measured over a total of 30−50 h), performed in most cases on at least two independent samples. In the step-scan measurements this resulted in a noise level of ∼15 μOD for *fast* cycles (i.e., tens of milliseconds) and ∼60 μOD for samples with *slow* cycles (in the hundreds of milliseconds). Kinetic data analysis was performed (mostly) by a nonlinear least-squares global fitting to multiexponentials using the program FITEXP (*28*, *29*). These fits yield the best approximation of measured data, $\Delta A(\nu_j,t)$, in the form

$$\Delta A(\nu_j,t) = \sum\{B_i(\nu_j, i)\exp[-t/\tau_i]\} + B_0$$

where τ_i are the time constants of kinetic processes and B_i-(ν_j, i) are the corresponding amplitudes of these processes. (That is, the time constant τ_i was constrained to be the same at all ν_j for the ith process.) The number of detected transient states was determined by applying *F*-test statistics (*29*, *30*). Prior to fitting, the data were condensed by averaging to a quasi-logarithmic time base with ∼13 time points per decade. The spectra were reconstructed from the amplitude spectra calculated from global fits to exponentials and are shown summed over all the preceding transitions. Thus, they refer to spectra extrapolated to the completion of the transition under consideration. In one case ([^{13}C]aspartate isotope effect), singular-value decomposition, SVD, was applied using the routine from Matlab (Ver. 4.2c.1, MathWorks, Inc., Natick, MA).

High-resolution solid-state 100.6 MHz ^{13}C NMR spectra were recorded in the dark at ambient temperature (20 °C) on a Chemagnetic CMX-400 NMR spectrometer by the cross polarization−magic angle spinning (CP-MAS) method. The spectral width, contact time, and acquisition time were 40 kHz, 1.5 ms, and 25 ms, respectively. Free induction decays were acquired with 1000 data points and Fourier-transformed as 8000 data points after 7K data points were zero-filled. Transients were accumulated 20 000−25 000 times. Difference spectra were recorded after line broadening. ^{13}C chemical shifts were referred to the carboxyl signal of glycine (176.03 ppm from tetramethylsilane) and then expressed as relative shifts. Aliquots of concentrated HCl solution were added stepwise to the samples to adjust appropriate pH. No buffer was used for the pH-titration study at acidic pH to avoid overlap of signals from buffer, except for the sample of pH 7 used for the peak assignment to which 5 mM HEPES buffer, 10 mM NaCl, and 0.025% NaN_3 were added. The samples were contained in a 5 mm o.d. zirconia rotor, and the caps for the rotor were tightly glued to the rotors to prevent leakage or evaporation of water from the hydrated samples under the stream of dry compressed air used for spinning.

RESULTS

Proton Release and Uptake during the Photocycles of Glu-194 and Glu-204 Mutants. The release of protons to the membrane surface and their appearance in the bulk medium can be followed during the photocycle by measuring the absorption changes of covalently bound fluorescein and pyranine in solution (*25*, *31*, *32*). In the wild-type protein near neutral pH, the release to the extracellular surface is more or less coincident with the deprotonation of the Schiff base. Fluorescein detects it on the surface at about 100 μs, while pyranine detects it in the bulk medium at 0.5−1 ms ("early release"). Uptake at the cytoplasmic surface occurs in several milliseconds. When the proton release mechanism is blocked, as in the wild type at or below pH 5 or in E204Q or R82Q, the photocycle reactions proceed further but the uptake on the cytoplasmic side occurs before the release (*10*, *16*, *33*). The appearance of net uptake at 10 ms or later, followed by the final release step ("late release"), is the indication of such a defect.

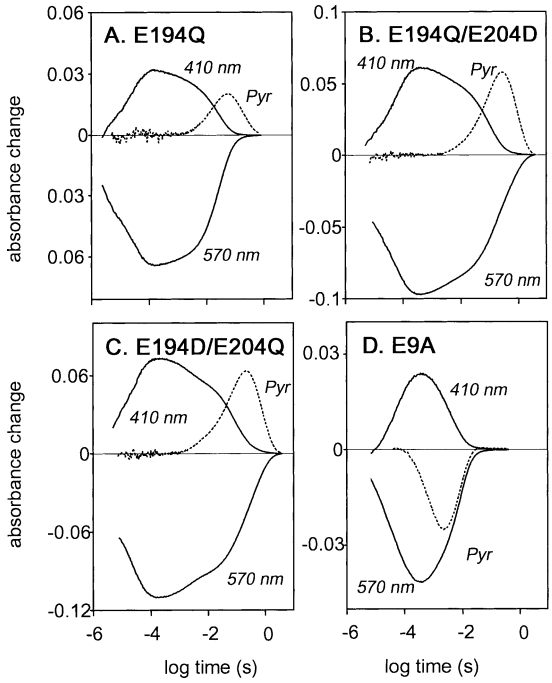

FIGURE 1: Deprotonation of the retinal Schiff base and proton kinetics in the photocycles of the E194Q (A), E194Q/E204D (B), E194D/E204Q (C), and E9A (D) bacteriorhodopsin mutants. The deprotonation of the Schiff base is measured as absorption increase at 410 nm, and the depletion of the initial state as absorption decrease at 570 nm. The pH changes in the bulk medium are followed by measuring absorption change from the indicator dye, pyranine, at 457 nm. Proton release is absorption decrease at this wavelength; uptake is absorption increase. Conditions: (A) 2 M NaCl, pH 6.9, 23 °C, pyranine trace shown 10× enlarged; (B, C) 0.15 M NaCl, pH 7.4, 15 °C, pyranine trace 5× enlarged; (D) 2 M NaCl, pH 6.5, 20 °C, pyranine trace 4× enlarged.

Figure 1 shows measurements using pyranine with the E194Q, E194D/E204Q, and E194Q/E204D, and E9A mutants. The proton kinetics of the first three of these proteins, as well as E194Q/E204Q (not shown), indicates complete absence of early release. According to these results, replacement of Glu-194 with a glutamine, either by itself or together with replacement of Glu-204 with either glutamine or aspartate, blocks proton release. This is consistent with the absence of early release in E194C (*19*) and similar to the case of the phenotype of E204Q (*10*, *11*, *33*). On the other hand, Figure 1D shows that the proton kinetics in the E9A mutant are like those in the wild type [compare with Figure 4 in ref 25]. Thus, mutation of Glu-9 has no effect on proton release.

Figure 2 shows proton and chromophore kinetics in E194D, as measured both with fluorescein covalently bound

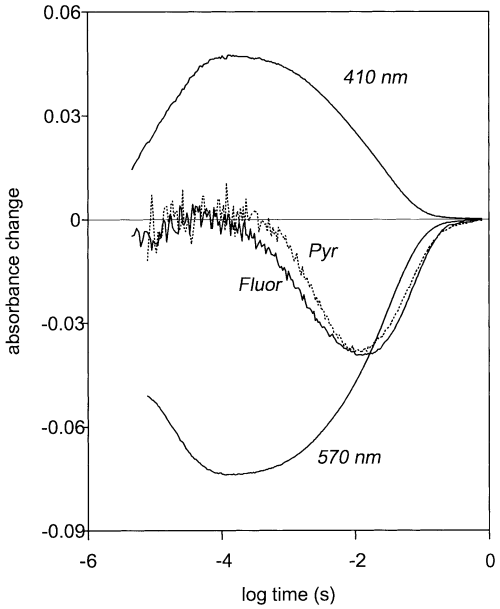

FIGURE 2: Chromophore and proton kinetics in the photocycle of the E194D mutant. Absorption changes at 410 and 570 nm are shown, as well as pH changes detected by fluorescein covalently linked to Lys-129 on the extracellular surface and by pyranine. Conditions: 0.15 M NaCl, pH 7.5, 15 °C. The fluorescein and pyranine traces are shown 20× and 17× enlarged, respectively.

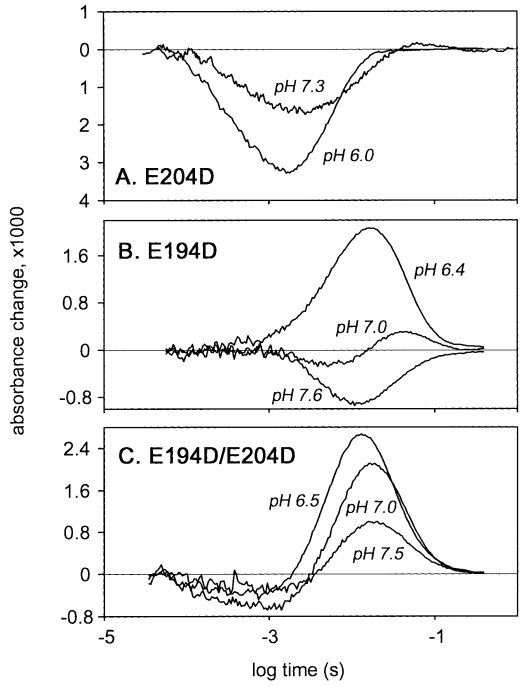

FIGURE 3: pH dependence of the proton kinetics in E204D (A), E194D (B), and E194D/E204D (C) as measured with pyranine. Proton release is absorption decrease; uptake is absorption increase. Conditions: 2 M NaCl, 20 °C.

to Lys-129 and with pyranine in the bulk. In this mutant, the proton release is observed, but with a considerably longer time constant than in the wild type ($\tau = 3.0 \pm 0.1$ ms under the conditions of the experiment, at 15 °C). It occurs much later than the deprotonation of the Schiff base, shown in Figure 2 as absorption increase at 410 nm (rise of the M state). In Figure 3, proton kinetics are shown for E204D, E194D, and E194D/E204D at various pH values between 6 and 7.5. In this pH range, E204D (Figure 3A) behaves

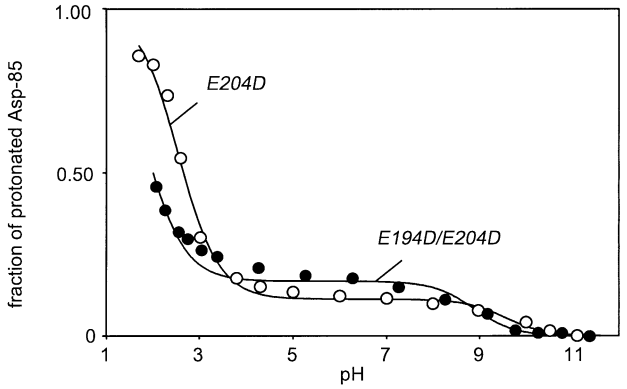

FIGURE 4: Spectroscopic titration of Asp-85 in E204D and E194D/E204D bacteriorhodopsins. The fraction of protonated Asp-85 was calculated from the amplitudes of the difference spectra in the pH-dependent blue−purple equilibrium, as described in ref 13. Symbols: open circles, E204D; filled circles, E194D/E204D. The lines were drawn with the following pK_a values: for E204D, pK_a of Asp-85 is 2.6 when Asp-204 is protonated and 8.6 when anionic, pK_a for Asp-204 is 3.5 when Asp-85 is protonated and 9.5 when anionic; for E194D/E204D, pK_a of Asp-85 is 1.6 when Asp-204 is protonated and 7.9 when anionic, pK_a for Asp-204 is 2.3 when Asp-85 is protonated and 8.5 when anionic. Conditions: 1 M Na_2SO_4, 40 mM phosphate, 40 mM MES, 20 mM bis(Tris)propane, 20 mM CAPS.

approximately as the wild type. Since the pH is well above the pK_a for proton release but well below the pK_a of the release site in the unphotolyzed protein (*11*), proton release is almost normal although its amplitude varies with pH according to the pK_a's of pyranine and surface buffering groups. A small extent of net uptake in the 80 ms time region at pH 7.3 indicates that release is partly blocked at pH 7.3. The reason for this will be discussed below. In E194D (Figure 3B), release is observed at pH 7.6, but its significant blockage at pH 7.0 and the transition to net uptake at pH 6.4 indicate that the pK_a for proton release is increased to about 7 by the mutation. In E194D/E204D (Figure 3C), the transition from net release to net uptake is absent. Release and uptake are seen together in the entire pH range between 6.5 and 7.5. The reason for this unique and unexpected behavior will be discussed below.

Influence of Residue 194 on the Coupling of the pK_a's of Asp-85 and Residue 204. The interaction of the proton release group with Asp-85 results in biphasic titration of the aspartate. This could be observed in the wild-type protein and in various mutants with shifted pK_a's, but not in E204Q, by measuring the rate of retinal isomeric equilibration in the dark or by directly measuring the blue-to-purple spectral shift when Asp-85 deprotonates (*11*−*13*, *34*, *35*). We used the more direct spectrophotometric titration except when the interacting pK_a's were far apart, as in the wild type, and the higher pK_a was difficult to observe. A problem with E194Q was that in any case it did not exhibit dark adaptation. Where possible, we carried out the spectral titrations instead. Glu-194 mutants that contain also the E204D residue replacement are well suited for such experiments because the E204D mutation makes the biphasic shape of the spectral titration curves very obvious (*11*).

Figure 4 shows spectrophotometric titration of E204D and E194D/E204D. The appearance of unspecified blue-shifted species that interfere with these measurements in the Glu-194 mutants was eliminated by including 1 M Na_2SO_4 in

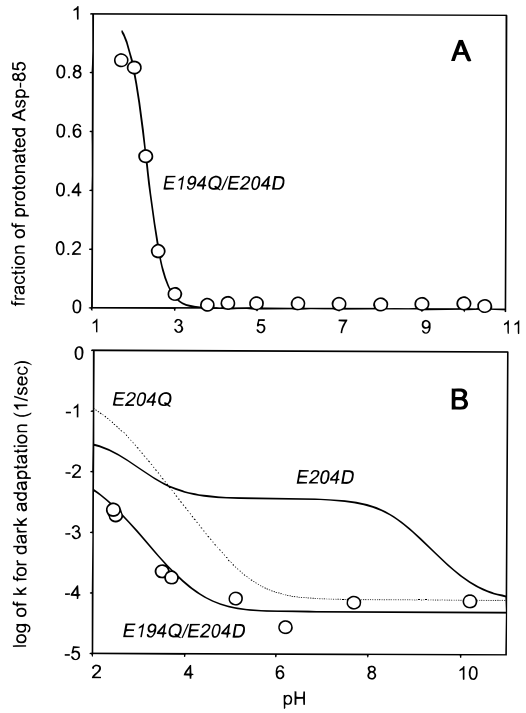

FIGURE 5: Direct and indirect titration of Asp-85 in E194Q/E204D: (A) spectroscopic titration, where the fraction of protonated Asp-85 is calculated from the blue-purple equilibrium (*13*) that makes the absorption at 650 nm (from the blue species) pH dependent; (B) indirect titration, by determining the rate constant for dark adaptation (*34*). Also included are the corresponding curves for E204D (solid line) and E204Q (dashed line) from ref 11. Conditions are as in Figure 4.

the solutions. The lines in Figure 4 represent the best fits of the Asp-85/Glu-204 interacting pair model (*35*). The four pK_a's of E204D under the conditions used, and of E194D/E204D, are somewhat changed but remain within 1 pH unit of those calculated earlier for E204D from the rates of dark adaptation (*11*). The pK_a of Asp-85 strongly increases when the interacting residue deprotonates, and conversely, the pK_a of the interacting residue strongly decreases when Asp-85 protonates. The result is the anomalous titration of Asp-85, with two apparent pK_a's and therefore a substantial amount of protonated Asp-85 near neutral pH. We conclude from Figure 4 that this interaction is not strongly affected when Glu-194 is replaced with an aspartate.

Replacement of Glu-194 with a glutamine has a more drastic effect. Figure 5A shows that spectroscopic titration of the E194Q/E204D mutant reveals only one pK_a. While this represents a large difference from the titration curve of E204D (Figure 4), the diminished amplitude of the second deprotonation of Asp-85 does not rule out coupling. Measurement of the rates of dark adaptation allows detection of smaller amounts of protonated Asp-85 (*34*). Figure 5B shows this kind of data for E194Q/E204D, together with the corresponding curves for E204D and E204Q from ref 11 (note that the ordinate is on a logarithmic scale). It is evident from Figure 5B that the E194Q replacement eliminates the biphasic titration of Asp-85, signaling that coupling of this aspartate with the proton release site is abolished, as in the E204Q (*11*) and E194C (*19*) mutants.

FTIR Spectra of the Photointermediates of E194D. Figure 6 shows a series of FTIR spectra measured at selected times after photoexcitation of the E194D mutant. As discussed

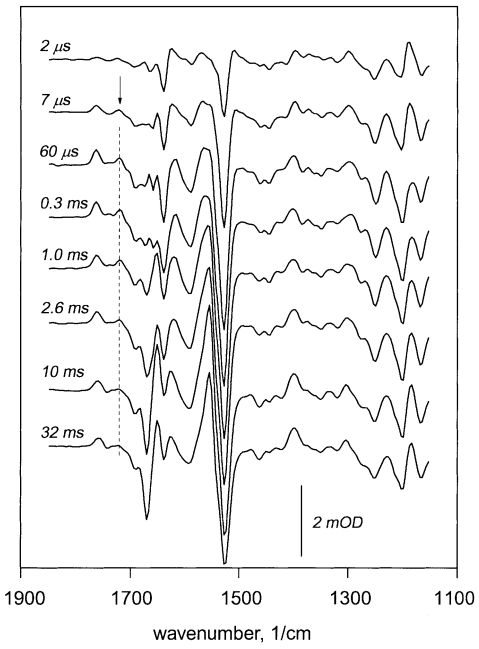

FIGURE 6: FTIR difference spectra at selected times after flash excitation of E194D. The pH was 8.5. The first four traces were measured with 5 μs resolution; the last four were measured with 50 μs resolution and with a different sample.

below, the first spectrum contains mostly the L intermediate. The L to M conversion is evident from the appearance of the positive band of the C═O stretch of the protonated Asp-85 at 1762 cm^{-1}, a positive ethylenic stretch band at 1560 cm^{-1}, which accompanies the corresponding prominent depletion band at 1527 cm^{-1}, and the shift of the positive 1186 cm^{-1} C−C stretch band of the 13-cis isomeric retinal to below the baseline (*2*, *36*). The bands characteristic of M, established by tens of microseconds, remain present until several milliseconds. The shift of the 1762 cm^{-1} band to a lower frequency, the shift of the 1186 cm^{-1} band to above the baseline, and the appearance of the large negative/positive pair of amide I bands at 1670/1650 cm^{-1} indicate that by 10 ms the N intermediate dominates the spectrum.

To ensure that the films used for FTIR measurements are equivalent to the membrane suspensions used in visible spectroscopy, we compared the photocycle kinetics in these samples. Table 1 shows the time constants obtained from global fitting of three sets of time-resolved measurements at pH 6.0: (a) absorption changes of membrane suspensions, at 570, 410, and 660 nm, (b) absorption changes of films prepared for FTIR spectroscopy, at 570, 410, and 640 nm, and (c) FTIR spectra, between 1850 and 1100 cm^{-1}, of films. Reassuringly, the six time constants, for which values could be determined from both visible and FTIR measurements, are very similar. τ_1, τ_2, and τ_3 refer to the L to M conversion ($\sim$2, $\sim$20, and $\sim$70 μs), τ_4 and τ_5 to the M to N conversion ($\sim$0.5 and $\sim$4 ms), and τ_6 and τ_7 to the recovery of the initial state ($\sim$16 and $\sim$40 ms), but the precise assignment of these time constants is not the objective of this study. In the visible the amplitudes associated with τ_3, τ_4, and τ_7 are much lower than the others, and in the infrared the same can be said of the amplitudes for the τ_4 and τ_7 processes. Thus, roughly speaking, at pH 6.0 the time constants τ_1, τ_2, τ_3, τ_5, and τ_6 describe the photocycle. Figure 7 shows amplitude spectra from the FTIR measurements, extrapolated to the time before

Table 1: Time Constants from Global Fits of the Photocycle Reactions of E194D at pH 6.0 in Membrane Suspension and in Hydrated Film, Measured with Visible and FTIR Spectroscopy[a]

	visible, membrane suspension	visible, hydrated film	FTIR, hydrated film
τ_1 (μs)	2	~4	ND
τ_2 (μs)	18 ± 0.3	20 ± 0.6	17 ± 0.2
τ_3 (μs)	76 ± 9	140 ± 60	70 ± 20
τ_4 (ms)	0.6 ± 0.2	1.1 ± 0.3	0.5 ± 0.2
τ_5 (ms)	3.8 ± 0.2	5.4 ± 0.3	4 ± 1
τ_6 (ms)	16 ± 0.2	15.5 ± 0.2	18 ± 2
τ_7 (ms)	43 ± 3	70 ± 30	50 ± 20

[a] The number of valid exponentials was determined with *F*-test statistics (see Materials and Methods). For measurements in the visible, the risk factor was negligible for the first seven exponentials, but increased 16× and 120× for including an eighth component for the FTIR film and the membrane sample, respectively. The same analysis was done for measurements in the infrared in separate rapid and slow time base step-scan experiments, which provided the first three and the second two exponentials, respectively, with risk factors increasing 100−600× for an additional component. The last time constant was obtained from rapid-scan measurements.

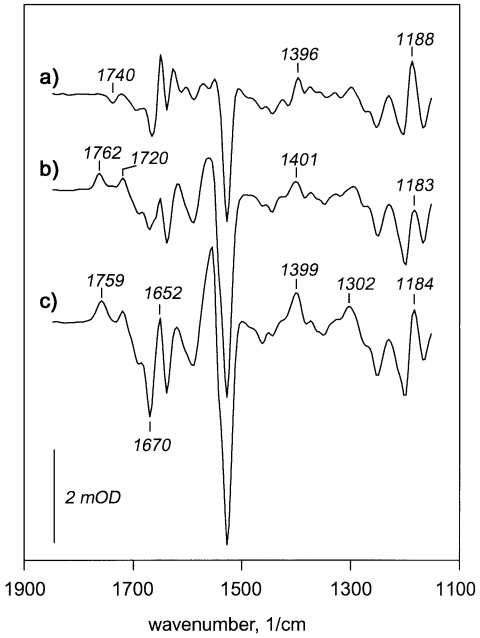

FIGURE 7: Amplitude spectra for E194D, from global fitting of FTIR difference spectra at pH 6.0. Trace a is extrapolated to the time before the τ_2 process and corresponds to the L minus BR spectrum. Trace b is after the process described τ_3 is completed (cf. Table 1) and corresponds to the M minus BR spectrum. Trace c is after the process described by τ_6 is completed (cf. Table 1) and corresponds to the (M plus N) minus BR spectrum.

τ_2, (the τ_1 process not being resolved), corresponding mainly to the L state (a), and after the processes described by τ_3 and τ_5 were completed, corresponding to the M (b) and N (c) states (or their mixtures), respectively. These spectra are very similar to earlier reported FTIR spectra for L, M, and N (*2*, *8*, *36*). Briefly, L minus BR spectra are recognized from a negative band at 1740 cm^{-1} from perturbation of Asp-96 and Asp-115 and from an intense C−C stretch band at 1186 cm^{-1}. M minus BR spectra contain, besides the 1762 cm^{-1} band of the protonated Asp-85, an increased negative ethylenic stretch band and lowered intensity for the 1183 cm^{-1} C−C stretch. In the N minus BR spectra, the Asp-85 band is shifted to 1755 cm^{-1} and the intensity of the 1302

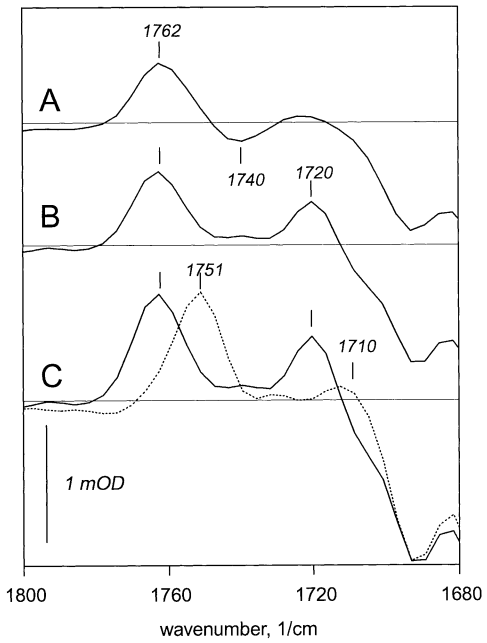

FIGURE 8: FTIR difference spectra for wild-type bacteriorhodopsin (A) and the E194D mutant (B, C). The spectra are calculated from global fits and consist of the photointermediate minus BR spectrum after completion of the L to M transition. In part C, the spectrum with H_2O is shown by a solid line and that with D_2O by a dotted line. The pH was 7.0.

cm^{-1} band and particularly that of the 1184 cm^{-1} band are increased. In view of its differences from spectrum b, spectrum c in Figure 7 appears to be a mixture of spectra for the M and N intermediates. With some conspicuous exceptions, the spectra in Figures 6 and 7 are very similar to what is seen for the wild type. One of these exceptions is an unusual shift of the positive band near 1400 cm^{-1} between the L minus BR and M minus BR spectra toward higher frequency (Figure 7). This band contains contributions from symmetric C═O stretch and from the N−H bend of the Schiff base (*36*). It is not clear why this band shifts in the spectrum of E194D and not in that of the wild type.

The main difference of the E194D mutants from wild type, however, is a positive band at 1720 cm^{-1}. The experiments below were intended to further describe this band, indicated with an arrow in Figure 6 and labeled in Figure 7, spectrum b). A spectrum for the wild type after completion of the M rise is given in Figure 8A in the expanded 1680−1800 cm^{-1} frequency region. It contains the C═O stretch of the protonated Asp-85 at 1762 cm^{-1} and a small, broad negative band near 1740 cm^{-1} that originates from perturbation or deprotonation of Asp-96 and Asp-115 in the L and N intermediates (*6*, *37*−*39*). In the equivalent spectrum of the E194D mutant (Figure 8B), the Asp-85 band is unchanged, the 1740 cm^{-1} band seems to be absent, and a prominent positive band at 1720 cm^{-1}appears. The last is specific for E194D and is not observed in the spectra of either E204D (*10*) or other bacteriorhodopsin samples studied before. Bands in the 1700−1800 cm^{-1} region are usually assigned to the C═O stretch of a protonated aspartate or glutamate. Isotope effects helped to assign the 1720 cm^{-1} band more specifically. It is shifted, as is the 1762 cm^{-1} band, by 10−11 cm^{-1} toward lower frequencies when the H_2O is replaced with D_2O (Figure 8C), consistent with the deuterium isotope

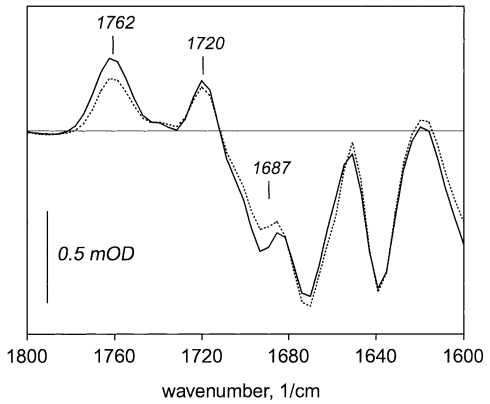

FIGURE 9: [^{13}C]Aspartate isotope effects in E194D. The spectrum with unlabeled aspartate is shown by a solid line, and the one with partial [4-^{13}C]aspartate is shown by a dotted line. The small differences required extraordinary measures to increase signal/noise and reproducibility. Unlike all the others, the spectra were measured with partly hydrated films at 5 °C and with rapid scans rather than step scans. They are shown after reconstruction from SVD spectra and scaling together to the amplitude of the negative ethylenic stretch band at 1527 cm^{-1}. The pH was 7.0.

effect on the C═O stretch of protonated carboxyls. Partial replacement of the aspartates with [4-^{13}C]aspartate was accomplished by growing the E194D cells in a synthetic medium containing the side chain C═O labeled amino acid. Figure 9 shows that about 25% of the amplitude of the 1762 cm^{-1} band is shifted to a lower frequency. From the expected approximately 40 cm^{-1} downshift in this kind of isotopic labeling (*40*, *41*), the shifted band should overlap the 1720 cm^{-1} band, while part of the latter should be shifted to about 1680 cm^{-1}. This is indeed observed, although the amplitude increase is maximal near 1687 cm^{-1} rather than at 1680 cm^{-1} (Figure 9). The two isotope effects positively identify the 1720 cm^{-1} band as originating from a protonated aspartate. Since a corresponding negative band is not seen in these spectra, the positive band arises most likely from protonation of the carboxylate of the aspartate rather than from a shift due to environmental change.

Parts A and B of Figure 10 show the rise kinetics of the 1762 cm^{-1} and 1720 cm^{-1} bands and the decay kinetics of the latter, respectively. The data in panel A indicate that the formations of the 1762 and 1720 cm^{-1} bands are similar. Global fitting of all the FTIR amplitudes in the 1850−1100 cm^{-1} frequency range yielded two time constants for the L to M transition (τ_2 and τ_3 in Table 1). The rises of both the 1762 and 1720 cm^{-1} bands contain both of these time constants although with different weights (given in the legend to Figure 10). The rises of the two bands are therefore correlated and coincide approximately with the rise of the M state (Table 1). The rise kinetics of the 1720 cm^{-1} band is little affected by pH between 5 and 9, similarly to the rise of M (not shown). Its decay at pH 8 (4.5 ± 0.8 ms in Figure 10B) is coincident with the release of a proton to the surface, as detected by fluorescein and pyranine (time constant for fluorescein, 3.0 ± 0.1 ms in Figure 2). At pH 6 (and at pH <6, not shown), however, the decay of the 1720 cm^{-1} band is much slower (Figure 10B). Its time constant at pH 6.0 is 22 ± 1 ms. At this pH, it decays coincident with the last step in the photocycle with significant amplitude (τ_6 in Table 1), consistent with the observation that at pH <7 the proton

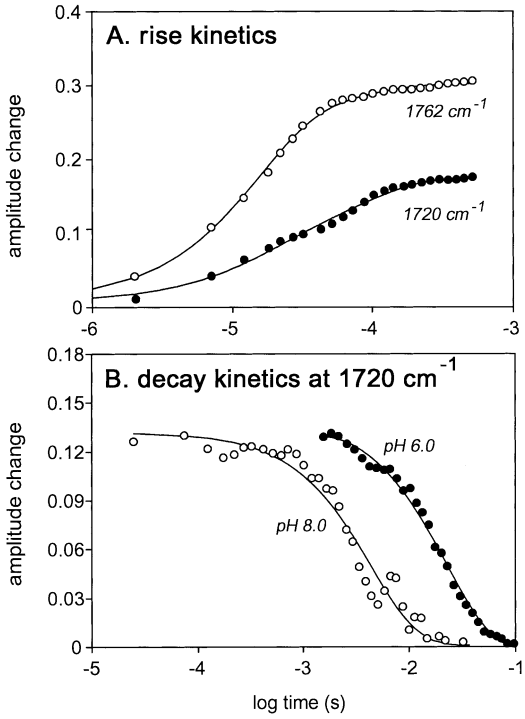

FIGURE 10: Kinetics of the rise and decay of the 1720 cm^{-1} band of E194D at pH 6.0. In (A) the rise kinetics are shown together with those of the 1762 cm^{-1} band (open circles). The time constants of formation are 16 ± 4 and 80 ± 20 μs, with fractional amplitudes of 0.31 and 0.69 for the 1720 cm^{-1} band and 0.86 and 0.14 for the 1762 cm^{-1} band. In (B) the decay of the 1720 cm^{-1} band is shown at pH 6.0 (closed circles) and 8.0 (open circles). The single time constants for the decay under the two conditions are 22 ± 1 and 4.5 ± 0.8 ms, respectively.

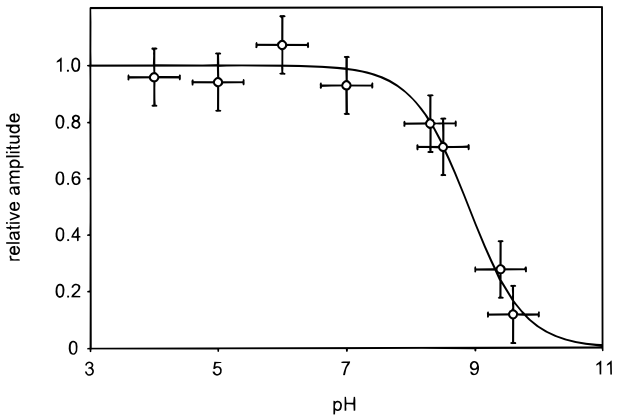

FIGURE 11: pH dependence of the amplitude of the 1720 cm^{-1} band of E194D. To correct for sample-to-sample variations, the amplitudes were normalized to the 1762 cm^{-1} band of the protonated Asp-85 that is invariant in this pH region. The amplitudes are shown normalized to 1 when extrapolated to low pH.

release is also shifted to the end of the photocycle (Figure 3B).

The pH dependence of the amplitude of the 1720 cm^{-1} band of the E194D mutant is shown in Figure 11. The amplitude declines with increasing pH. The error bars indicate the uncertainty in the amplitudes (determined mostly by baseline variations in the FTIR spectra) and in the pH (determined by drift of the pH during drying). The final pH was checked by comparing the decay kinetics of the films and membrane suspensions in the visible (cf. Table 1). The apparent pK_a is 8.9 ± 0.4. The pH dependence of the 1720

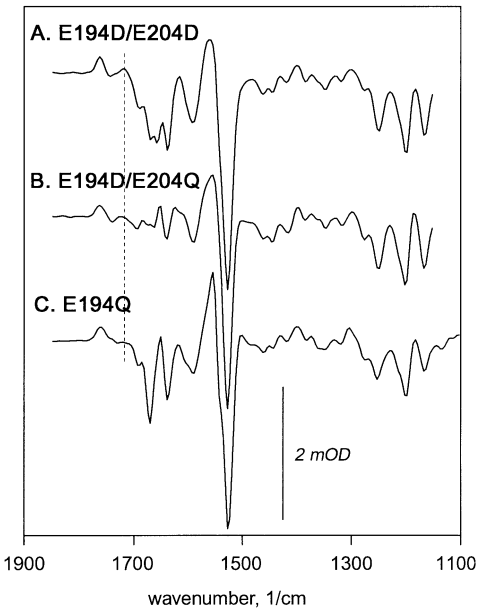

FIGURE 12: FTIR difference spectra of intermediate(s) after the L to M transition in E194D/E204D (A), E194D/E204Q (B), and E194Q (C). See text for details. The amplitudes were scaled to the negative ethylenic stretch frequency at 1527 cm^{-1} for the comparison. The position of the 1720 cm^{-1} band is indicated.

cm^{-1} band could not be determined in E194D/E204D because its amplitude in this mutant is much smaller (cf. below). Qualitatively, it also appeared to decline with increasing pH but with an apparent pK_a considerably lower than in E194D because at pH 8 the band was absent (not shown).

FTIR Spectra of the Photointermediates of E194D/E204Q, E194Q, and E194D/E204D. Figure 12 shows cumulative amplitude spectra after completion of the rise of the M intermediate of mutants in which either Glu-194 or Glu-204 is replaced with glutamine. Besides bands for the main component M, these spectra contain bands for other intermediates. In E194D/E204Q and E194Q, inhibition of proton release is expected to result in significant amounts of the L state in the L/M equilibrium (*16*). This is indeed shown by the positive 1186 cm^{-1} band in the C−C stretch region. In the spectrum of E194Q, the 1670 cm^{-1} amide I band indicates the presence of also N in this mixture. Nevertheless, from comparison with the 1762 cm^{-1} band of the protonated Asp-85 in the spectra for E194D/E204Q (A) and E194D/E204D (B), we can conclude that the 1720 cm^{-1} band arises when residue 204 is an aspartate but not when it is a glutamine. In fact, at no time in the photocycle does the 1720 cm^{-1} band appear in the spectra of these mutants. The band is smaller for E194D/E204D than for E194D (compare with Figures 6 and 7B), but for E194D/E204Q it is absent, this region being virtually identical with the spectrum of the wild type (compare with Figure 7A). The results indicate therefore that protonation of Asp-194 occurs only when residue 204 is either a glutamate or an aspartate. As expected from its assignment, the 1720 cm^{-1} band is absent also when residue 194 is a glutamine (Figure 12C).

NMR Titration of Asp-194. Figure 13A shows CP-MAS NMR spectra of [4-^{13}C]aspartate-labeled E194D (trace a) and wild type (trace b), both recorded at pH 7.0. The ^{13}C NMR signals of the wild type (b) are split into at least eight peaks that are very close to those reported by Engelhard et al. (*42*, *43*). Some peaks, especially those that resonate at 175.8 and 174.2 ppm, are doubled in the present spectrum, probably because hydrated pellets instead of lyophilized or hydrated lyophilized samples were used. The ^{13}C NMR signal of Asp-194 was unambiguously located at 178.4 ppm as indicated by an arrow, on the basis of the difference spectrum (a) − (b), illustrated in (c). This peak position corresponds to a deprotonated aspartate and remains unchanged from pH 7 to 4, as shown in the pH-titration curve of signal. The resonance of the label shifted upfield by 3 ppm to 175.4 ppm at pH 2, corresponding to the protonated state in the low-pH region, as expected from protonation of the carboxyl group in model peptides (*42*). The pK_a of Asp-194 was thus estimated as 3.0 directly from the pH-titration curve in Figure 13B. Since the salt concentration in the NMR experiment had to be kept lower than the usual concentration used, this pK_a is somewhat higher than what would be measured in 100 mM NaCl. We also examined ^{13}C NMR spectra of these samples by DD-MAS without cross polarization to be able to preferentially record ^{13}C NMR signals from the aspartate residue(s) on the mobile C-terminal tail (*44*, *45*). The pK_a detected at the C-terminus was very close to that of a free aspartic acid (4.2, not shown).

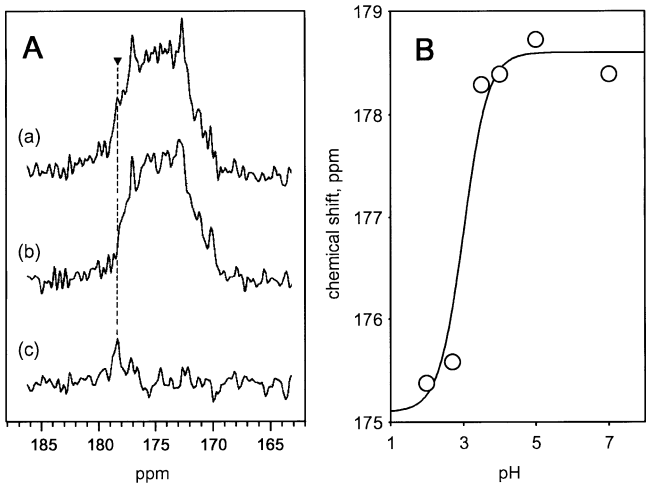

FIGURE 13: Solid-state NMR titration of Asp-194 in E194D: (A) CP-MAS NMR spectra for [4-^{13}C]aspartate labeled E194D (a) and wild-type (b) bacteriorhodopsins and the difference between them (c) at pH 7.0; (B) chemical shift of the Asp-194 peak in (c) as a function of pH.

DISCUSSION

The absence of proton release to the medium upon protonation of Asp-85 in the E194Q, E194Q/E204D, and E194Q/E204Q mutants indicates that the carboxyl group of Glu-194 is an essential part of the extracellular proton release machinery, as the carboxyl of Glu-204 was shown to be earlier (*10*). For proton release to occur, neither residue may be a glutamine (Figure 1A−C). On the other hand, Glu-194, as Glu-204, can be replaced with an aspartate without loss of function.

As for the proton release, the coupling between the pK_a's of Asp-85 and the proton release group requires that neither Glu-204 nor Glu-194 be a glutamine (ref 11, Figure 5), although they can be replaced with an aspartate. This unexpected finding confirms recent results with E194C (*19*) and strongly suggests that Glu-194 and Glu-204 also interact

but by itself does not reveal which residue is responsible for the coupling with Asp-85. Glu-204 is a better candidate because it is located between Asp-85 and Glu-194 (cf. below).

The functional roles of Glu-194 and Glu-204 do not appear to be the same. Which interacts with Asp-85 and which releases the proton to the surface? In the E194D/E204D mutant, the group that directly interacts with Asp-85 cannot be the proton release site, because its pK_a when Asp-85 is protonated is 2.3 (Figure 4), while the pK_a for proton release is not much lower than 7 (Figure 3C). Further, relative to the wild type, the pK_a for proton release is notably increased in E194D but not in E204D (Figure 3). In E194D, but again not in E204D, the time course of the release is delayed from about 150 μs in the wild type[2] to 3 ms. These results implicate residue 194 more than residue 204 as the terminal release site but not necessarily as the source of the released proton. For E194D, an FTIR band arises that is kinetically correlated with the protonation of Asp-85. It decays coincidently with the proton release to the surface. Its frequency, at 1720 cm^{-1} (Figures 6−9), and the observed D_2O and ^{13}C isotope effects indicate that this is a C═O stretch band that arises as the result of the protonation of an aspartate. The band is unique to E194D and E194D/E204D. There are no other aspartate residues in the extracellular region except Asp-85 and Asp-212. The 1720 cm^{-1} band cannot originate from either of these residues, since protonation of Asp-85 produces the 1762 cm^{-1} band, and protonation of Asp-212 would have drastic effects on the photocycle (*46*). Therefore, the results suggest that the additional aspartate that becomes protonated in E194D is Asp-194. The discussion below assumes that this is so.

The proton gained by Asp-194 does not originate from the medium, since fluorescein covalently bound to the surface has sufficient time resolution to detect a pH change between 10 and 100 μs (*25*, *31*, *32*), and none is observed (Figure 2). What is the internal proton donor? Deprotonations of Glu-204 and Asp-204 in the photocycle have been associated with negative C═O stretch bands at 1703 and 1713 cm^{-1}, respectively, but with rather small amplitudes (*10*) and poorly resolved or unresolved kinetics at cryogenic temperatures. We see no evidence of this kind of depletion of a protonated carboxyl group in either E194D or E194D/E204D. Part of the reason may be the lesser resolution (8 cm^{-1}) in our measurements. Another reason may be that, although it depends on Glu-204, the proton is only partly localized at the carboxyl group as we suggested before (*10*). On the other hand, the pH dependence of the protonation of Asp-194 (Figure 11) is consistent with the Glu-204 site as the source of the proton. The apparent pK_a of the amplitude of the 1720 cm^{-1} band must refer to the proton donor. At pH higher than its pK_a, the donor will be unprotonated in the unphotolyzed state and cannot provide a proton during the photocycle. Significantly, the observed pK_a of about 9 is about the same as the pK_a derived earlier for the group that serves as the source of the proton to be released (*17*) and for the Glu-204 site in the anomalous titration of Asp-85 (*11*, *35*). Thus, the proton donor to Asp-194 is very likely the Glu-204 site.

[2] At 15 °C, from ref 25.

This interpretation of the behavior of Glu-194 mutants made several predictions that were readily tested. First, if the 1720 cm^{-1} band reflects the protonation of Asp-194, and Glu-204 is the proton donor, the band should not arise for the E194D/E204Q mutant. This is indeed what was observed (compare Figures 6−9 with Figure 12B). Second, if the proton released to the surface is from the deprotonation of Asp-194, the dissociation should not occur below the pK_a of this group, which is about 7 (Figure 3B). At pH <7, proton release is delayed until the end of the photocycle, and the decay of the 1720 cm^{-1} band should be likewise delayed. This is indeed the case: while at pH 8 the decay of the 1720 cm^{-1} band has a time constant of about 4 ms, at pH 6 the decay occurs later (τ = 22 ms in Figure 10B) and coincidently with the proton release at the end of the photocycle at this pH (Figure 3B). Third, if the protonation of Asp-194 is to occur at pH as low as 4 (Figure 11), this residue must be anionic; i.e., its pK_a must be lower than 4 in the unphotolyzed state. Indeed, titration of Asp-194 in [4-^{13}C]aspartate labeled E194D with solid state NMR indicates that its pK_a is about 3 (Figure 13). Fourth, if the pK_a for the proton donor to Asp-194 is lowered when Glu-204 is replaced by an aspartate (ref 11 and this study), and the pK_a for proton release is raised when Glu-194 is replaced by an aspartate (Figure 3B), in E194D/E204D the two pK_a's involved in the proposed proton release pathway will overlap and there should be no pH where the double mutant can release protons in the normal way. Proton release will be blocked at both low and high pH, because at pH ≤ 7 the release site (Asp-194) cannot dissociate, while at pH ≥ 8 the internal proton donor (Asp-204) is anionic and cannot provide a proton. Indeed, unlike in E194D, in E194D/E204D proton release is partially blocked at every pH in the pH range 6.5−7.5 (compare Figure 3B and Figure 3C). A lowered pK_a for residue 204 as a proton donor when it is an aspartate explains also why in E204D proton release begins to be partially blocked at pH 7.3 already (Figure 3A).

We note that this interpretation of the data requires that residue 204 be protonated and residue 194 be anionic near pH 7, and this is contrary to what was deduced from electron diffraction (*20*). The reason for the discrepancy is not yet clear. In the case of Glu-204, the reason may be that the proton is not fully localized on the carboxyl group but occupies a diffuse site, as suggested earlier on the basis of the low amplitude of the C═O stretch depletion band (*10*). In the case of Glu-194, the difference may be between the aspartate in E194D and the glutamate in the wild type. However, it seems unlikely that environments of Asp-194 and Glu-194 would be so different as to change the pK_a to the required large extent. More direct methods of determining the pK_a's of the two glutamates, such as the NMR titration we report here, will decide this issue. The low pK_a found for Asp-194 is unexpected. Its origin could be hydrogen-bonding of its anionic form with Asn-76, located nearby on the B−C interhelical loop (*20*).

We propose that in the E194D mutant the protonation of Asp-194 by the Glu-204 site is triggered by the proton transfer from the Schiff base to Asp-85. The subsequent deprotonation of Asp-194 is considerably slower than its protonation, and therefore the protonated Asp-194 accumulates transiently and becomes observable by FTIR spectroscopy (Figures 6−9). Its deprotonation is coincident

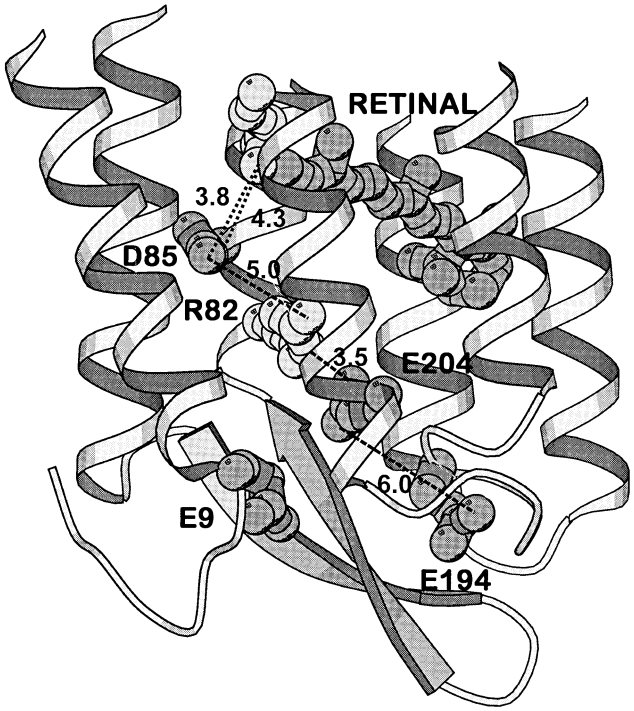

FIGURE 14: Structure of the extracellular region of bacteriorhodopsin, at 3 Å resolution (*20*, *48*). Only the extracellular half of the backbone, the retinal, and the side chains of residues discussed in this report are shown. Distances are given in angstroms. With the surface defined from the positions of the N and O atoms in residue side chains (*20*), even residues Glu-9, Glu-194, and Glu-204 are at least partly buried inside the protein.

with the protonation of fluorescein and pyranine, suggesting that the proton is released to the surface directly from Asp-194. Does this mechanism apply to Glu-194 in the wild type? On one hand, an FTIR band from Glu-194 is not observed, but this is expected from the fact (*25*, *31*, *32*, *47*) that the proton is detected at the surface on the same time scale as the protonation of Asp-85. Because its deprotonation is rapid relative to its protonation, the protonated state of Glu-194 could not accumulate. On the other hand, one must be careful in drawing conclusions about the wild type from mutants, and the negative result does not exclude the possibility that when residue 194 is a glutamate it does not participate in proton transfer. We are influenced against this alternative by the observations that proton release is abolished in E194Q and its pK_a is modified in E194D, even though these residue replacements should be minimally disruptive of the structure. We suggest therefore that in the wild-type protein Glu-194 functions in the same way as Asp-194 in E194D. According to this mechanism *the proton release depends on the sequential interaction of the Schiff base, Asp-85, Glu-204, Glu-194, arranged in a chain that leads to the extracellular surface*. The connection between Asp-85 and Glu-204 is through the coupling of their pK_a's described before (*11*, *12*), while the Glu-204 and Glu-194 constitute a proton donor/acceptor pair. The final event is the release of a proton to the surface by dissociation of Glu-194.

Figure 14 shows the structure of the extracellular region of bacteriorhodopsin, determined with electron diffraction at 3 Å resolution (*20*, *48*). Lys-216 with all-trans retinal, Asp-85, Arg-82, Glu-204, Glu-194, and Glu-9 are shown. The first five of these residues appear to form a connected pathway from the retinal Schiff base to the surface (*48*), consistent with the results that indicate their interaction. None of the distances along this chain, given in Figure 14, allow hydrogen bonds to form for facilitating proton transfer (*49*). Such bonds could form only if the conformation changed during the photocycle or water were intercalated between the residues either in the unphotolyzed state or in the photointermediates. At the resolution available in this structure it is not clear where water molecules are located, but there is extensive FTIR evidence for changes of water in this region of the protein during the photocycle (*50*). On the other hand, the existence of an icelike hydrogen-bonded chain that extends between the Schiff base and the surface (*51*, *52*) is ruled out in the unphotolyzed state by the recent 2.5 Å resolution X-ray diffraction structure (*53*) in which only a few water molecules are located in this region. The side chains of Asp-85, Arg-82, and Glu-204 face into this putative proton channel, but Glu-194 is turned about 90° toward the extracellular surface. This would not necessarily interrupt the proton conduction pathway provided that the local conformation is changed during the photocycle to better orient the COOH group for first accepting a proton from Glu-204 and then releasing it to the aqueous medium. Glu-9 is not much farther from this pathway than Glu-194 (8.1 Å from Glu-204, not shown in Figure 14, vs the 6.0 Å distance between Glu-194 and Glu-204), but the results we report (Figure 1D) rule it out as the terminal proton release site.

The two pK_a's earlier determined for the "proton release site", about 5 and about 9, thus refer to the Glu-204 site within the proton transfer chain rather than to Glu-204 as the proton release group. This requires some revision of the way the two pK_a's in the titration of Asp-85 are to be interpreted. The higher pK_a determines the protonation state of the Glu-204 site in the unphotolyzed protein, as suggested before, but the lower one is not for proton release to the surface. Rather, it is for the Glu-204 site at the time in the photocycle after Asp-85 became protonated. At pH above the higher pK_a, the proton donor Glu-204 site is anionic and the chain is interrupted. At pH below the pK_a for release, Glu-194 does not dissociate. It now appears that at such low pH the internal proton transfers may proceed as far as Glu-194, and the proton release that is observed at the end of the cycle (*16*) is not from Asp-85 directly, as previously thought, but from this residue. Under these conditions, Asp-85 protonates Glu-204 instead of releasing its proton to the surface. In one way or another, however, once the low pK_a of Asp-85 is reestablished at the end of the photocycle, its proton will be released to the surface even when residues 204 and 194 cannot mediate it. The observation of slow proton release at the end of the photocycle in E204Q/E194Q indicates the existence of an alternative pathway to the surface.

REFERENCES

1. Mathies, R. A., Lin, S. W., Ames, J. B., and Pollard, W. T. (1991) *Annu. Rev. Biophys. Biophys. Chem. 20*, 491−518.
2. Rothschild, K. J. (1992) *J. Bioenerg. Biomembr. 24*, 147−167.
3. Oesterhelt, D., Tittor, J., and Bamberg, E. (1992) *J. Bioenerg. Biomembr. 24*, 181−191.
4. Ebrey, T. G. (1993) in *Thermodynamics of membranes, receptors and channels* (Jackson, M., Ed.) pp 353−387, CRC Press, New York.
5. Lanyi, J. K. (1993) *Biochim. Biophys. Acta 1183*, 241−261.

6. Braiman, M. S., Mogi, T., Marti, T., Stern, L. J., Khorana, H. G., and Rothschild, K. J. (1988) *Biochemistry 27*, 8516−8520.
7. Bousché, O., Sonar, S., Krebs, M. P., Khorana, H. G., and Rothschild, K. J. (1992) *Photochem. Photobiol. 56*, 1085−1095.
8. Hessling, B., Souvignier, G., and Gerwert, K. (1993) *Biophys. J. 65*, 1929−1941.
9. Kandori, H., Yamazaki, Y., Hatanaka, M., Needleman, R., Brown, L. S., Richter, H. T., Lanyi, J. K., and Maeda, A. (1997) *Biochemistry 36*, 5134−5141.
10. Brown, L. S., Sasaki, J., Kandori, H., Maeda, A., Needleman, R., and Lanyi, J. K. (1995) *J. Biol. Chem. 270*, 27122−27126.
11. Richter, H. T., Brown, L. S., Needleman, R., and Lanyi, J. K. (1996) *Biochemistry 35*, 4054−4062.
12. Balashov, S. P., Imasheva, E. S., Govindjee, R., and Ebrey, T. G. (1996) *Biophys. J. 70*, 473−481.
13. Richter, H. T., Needleman, R., and Lanyi, J. K. (1996) *Biophys. J. 71*, 3392−3398.
14. Scharnagl, C., Hettenkofer, J., and Fischer, S. F. (1995) *J. Phys. Chem. 99*, 7787−7800.
15. Sampogna, R. V., and Honig, B. (1996) *Biophys. J. 71*, 1165−1171.
16. Zimányi, L., Váró, G., Chang, M., Ni, B., Needleman, R., and Lanyi, J. K. (1992) *Biochemistry 31*, 8535−8543.
17. Kono, M., Misra, S., and Ebrey, T. G. (1993) *FEBS Lett. 331*, 31−34.
18. Richter, H. T., Needleman, R., Kandori, H., Maeda, A., and Lanyi, J. K. (1996) *Biochemistry 35*, 15461−15466.
19. Balashov, S. P., Imasheva, E. S., Ebrey, T. G., Chen, N., Menick, D. R., and Crouch, R. K. (1997) *Biochemistry 36*, 8671−8676.
20. Kimura, Y., Vassylyev, D. G., Miyazawa, A., Kidera, A., Matsushima, M., Mitsuoka, K., Murata, K., Hirai, T., and Fujiyoshi, Y. (1997) *Nature 389*, 206−211.
21. Oesterhelt, D., and Stoeckenius, W. (1974) *Methods. Enzymol. 31*, 667−678.
22. Ni, B., Chang, M., Duschl, A., Lanyi, J. K., and Needleman, R. (1990) *Gene 90*, 169−172.
23. Onishi, H., McCance, M. E., and Gibbons, N. E. (1965) *Can. J. Microbiol. 11*, 365−373.
24. Brown, L. S., Váró, G., Needleman, R., and Lanyi, J. K. (1995) *Biophys. J. 69*, 2103-2111.
25. Cao, Y., Brown, L. S., Sasaki, J., Maeda, A., Needleman, R., and Lanyi, J. K. (1995) *Biophys. J. 68*, 1518−1530.
26. Govindjee, R., Balashov, S. P., and Ebrey, T. G. (1990) *Biophys. J. 58*, 597−608.
27. Chizhov, I. V., Engelhard, M., Sharkov, A. V., and Hess, B. (1992) in *Structure and Function of Retinal Proteins* (Rigaud, J. L., Ed.) pp 171−173, INSERM/John Libbey Eurotext, Inc., Paris.
28. Sharonov, A. Y., Tkachenko, N. V., Savransky, V. V., and Dioumaev, A. K. (1991) *Photochem. Photobiol. 54*, 889−893.
29. Dioumaev, A. K. (1997) *Biophys. Chem. 67*, 1−25.
30. Bevington, P. R., and Robinson, D. K. (1992) *Data reduction and error analysis for the physical sciences*, McGraw-Hill, New York.
31. Heberle, J., and Dencher, N. A. (1992) *Proc. Natl. Acad. Sci. U.S.A. 89*, 5996−6000.
32. Alexiev, U., Marti, T., Heyn, M. P., Khorana, H. G., and Scherrer, P. (1994) *Biochemistry 33*, 13693−13699.
33. Govindjee, R., Misra, S., Balashov, S. P., Ebrey, T. G., Crouch, R. K., and Menick, D. R. (1996) *Biophys. J. 71*, 1011−1023.
34. Balashov, S. P., Govindjee, R., Kono, M., Imasheva, E., Lukashev, E., Ebrey, T. G., Crouch, R. K., Menick, D. R., and Feng, Y. (1993) *Biochemistry 32*, 10331−10343.
35. Balashov, S. P., Govindjee, R., Imasheva, E. S., Misra, S., Ebrey, T. G., Feng, Y., Crouch, R. K., and Menick, D. R. (1995) *Biochemistry 34*, 8820−8834.
36. Maeda, A. (1995) *Isr. J. Chem. 35*, 387−400.
37. Gerwert, K., Hess, B., Soppa, J., and Oesterhelt, D. (1989) *Proc. Natl. Acad. Sci. U.S.A. 86*, 4943−4947.
38. Maeda, A., Sasaki, J., Shichida, Y., Yoshizawa, T., Chang, M., Ni, B., Needleman, R., and Lanyi, J. K. (1992) *Biochemistry 31*, 4684−4690.
39. Sasaki, J., Lanyi, J. K., Needleman, R., Yoshizawa, T., and Maeda, A. (1994) *Biochemistry 33*, 3178−3184.
40. Engelhard, M., Gerwert, K., Hess, B., Kreutz, W., and Siebert, F. (1985) *Biochemistry. 24*, 400−407.
41. Tadesse, L., Nazarbaghi, R., and Walters, L. (1991) *J. Am. Chem. Soc. 113*, 7036−7037.
42. Engelhard, M., Hess, B., Emeis, D., Metz, G., Kreutz, W., and Siebert, F. (1989) *Biochemistry 28*, 3967−3975.
43. Metz, G., Siebert, F., and Engelhard, M. (1992) *Biochemistry 31*, 455−462.
44. Tuzi, S., Yamaguchi, S., Naito, A., Needleman, R., Lanyi, J. K., and Saitô, H. (1996) *Biochemistry 35*, 7520−7527.
45. Tuzi, S., Naito, A., and Saitô, H. (1996) *Eur. J. Biochem. 239*, 294−301.
46. Needleman, R., Chang, M., Ni, B., Váró, G., Fornes, J., White, S. H., and Lanyi, J. K. (1991) *J. Biol. Chem. 266*, 11478−11484.
47. Scherrer, P., Alexiev, U., Marti, T., Khorana, H. G., and Heyn, M. P. (1994) *Biochemistry 33*, 13684−13692.
48. Kimura, Y., Vassylyev, D. G., Miyazawa, A., Kidera, A., Matsushima, M., Mitsuoka, K., Murata, K., Hirai, T., and Fujiyoshi, Y. (1997) *Photochem. Photobiol. 66*, 764−767.
49. Scheiner, S., and Duan, X. (1991) *Biophys. J. 60*, 874−883.
50. Maeda, A., Kandori, H., Yamazaki, Y., Nishimura, S., Hatanaka, M., Chon, Y. S., Sasaki, J., Needleman, R., and Lanyi, J. K. (1997) *J. Biochem. (Tokyo) 121*, 399−406.
51. Le Coutre, J., Tittor, J., Oesterhelt, D., and Gerwert, K. (1995) *Proc. Natl. Acad. Sci. U.S.A. 92*, 4962−4966.
52. Le Coutre, J., and Gerwert, K. (1996) *FEBS Lett. 398*, 333−336.
53. Pebay-Peyroula, E., Rummel, G., Rosenbusch, J. P., and Landau, E. M. (1997) *Science 277*, 1676−1681.

BI971842M